Energy Engineering

Tech Science Press

Doi:10.32604/ee.2026.073197

ARTICLE

Operation Optimization of Microgrid Clusters Coordinated with Distribution Systems with Limited Information Exchange

Qianfeng Wu[1], Dabo Xie[1], Wenhua Ni[2], Junjie Zhou[1], Xuantong Lu[1], Chengying Ma[1], Rongqiang Li[2,*] and Yang Li[2,*]

[1]Suqian Electric Power Design Institute Co., Ltd., Suqian, 223800, China
[2]School of Electrical and Power Engineering, Hohai University, Nanjing, 211100, China

*Corresponding Authors: Rongqiang Li. Email: 221606030022@hhu.edu.cn; Yang Li. Email: eeliyang@hhu.edu.cn

Received: 12 September 2025; Accepted: 29 December 2025; Published: 27 April 2026

ABSTRACT: With the deepening of the power system reform, an increasing number of microgrids are being integrated into the distribution network. In traditional centralized optimization algorithms, the optimal power flow model of the distribution network and the optimal scheduling model of microgrid clusters are directly coupled and solved simultaneously. This process involves extensive information exchange between the upper distribution network system and the lower microgrid clusters, which not only increases the communication burden but also prolongs computation time and raises computational complexity. Moreover, it requires excessive information sharing, making it difficult to achieve limited information exchange between the upper and lower systems. In this paper, an optimization model and solution method based on the analytical target cascading approach are proposed. First, a typical microgrid model is constructed. On this basis, a collaborative optimization model for the active distribution network (ADN) and microgrid clusters is established. The distribution network and the microgrid clusters are treated as a unified entity of interest, with their interconnection power represented as virtual generators and virtual loads to achieve decoupling. Finally, simulations based on the IEEE-33 node standard system are conducted. Compared with the centralized algorithm, the effectiveness of the analytical target cascading method in coordinating the distribution network and microgrid clusters is verified. The proposed approach reduces computational complexity and enables optimized operation with limited information exchange.

KEYWORDS: Distribution network; microgrid clusters; analysis target cascading; collaborative optimization; optimal scheduling; limited information exchange

1 Introduction

A microgrid is connected to the distribution network, and through the collaborative optimization among various energy sources, the energy utilization efficiency is improved, the phenomenon of wind power and photovoltaic abandonment is greatly reduced, the consumption rate of renewable energy, such as wind power and photovoltaic, is increased, the dependence on fossil energy is reduced, and carbon emission is reduced [1]. A microgrid compensates for the poor reliability of power supply from a single energy source by leveraging the complementarity of multiple energy sources, thereby improving power supply reliability. Due to the microgrid's flexibility, the distribution network can quickly respond to load changes, thereby improving the power grid's flexibility [2,3]. Vigorously developing the microgrid, continuously promoting the construction of the energy internet, establishing microgrid clusters, and realizing the sharing and intelligent management of energy information across various systems are the future development trends [4].

Currently, many studies focus on interactions between microgrids. Reference [5] discusses the optimal planning of dual-zero microgrids on islands, focusing on integrating renewable energy effectively while achieving carbon neutrality. Reference [6] proposes an adaptive risk-averse optimization method for multi-energy microgrids (MEMG), aiming to address the scheduling of electricity and thermal energy. Reference [7] introduces a risk-aware operation method for multi-energy microgrids, combining large language models and distributed Pareto-optimal reinforcement learning to deal with uncertainties in offshore multi-energy microgrids. Reference [8] presents a multi-stage scheduling strategy for microgrid resource clusters based on a hybrid data-driven approach. Reference [9] proposes a reputation-based, resilient distributed energy management method to enhance microgrid resilience against cyberattacks. Current research that focuses solely on microgrids has some limitations. Many studies overlook the potential benefits of coordination between microgrids and the distribution network, leading to inefficiencies in resource allocation and energy scheduling. For example, when microgrids operate independently, they miss opportunities to leverage support from neighboring microgrids or the broader distribution network, thereby compromising system stability. Furthermore, the lack of coordinated optimization often means that microgrid operations and demand management are not optimized at the network level. Integrating microgrids with the distribution network for coordinated optimization can lead to more efficient resource sharing, enhanced system stability, and improved cost-effectiveness.

The current mainstream approach for optimizing the scheduling of microgrid clusters connected to the distribution network relies on centralized algorithms. In this method, various operational constraints and limits of both the distribution network and microgrid clusters are integrated into a single model, and the optimal solution is obtained through a one-time optimization. Reference [10] compares cooperative and non-cooperative games, examines the benefit distribution in local energy trading amid increasing distributed resources, introduces virtual price leaders, and achieves fair benefit distribution. References [11,12] summarize the application of game theory in peer-to-peer transactions in smart grids and discuss its application in electric vehicles (EVs), distributed energy, and energy storage. Reference [13] proposes a two-stage stochastic optimization two-layer model for active distribution networks (ADNs) with multiple microgrids, effectively managing energy exchange between distribution networks and microgrids by accounting for both day-ahead and real-time decisions. Based on the Stackelberg game framework, reference [14] considers the uncertainty in microgrids and adopts a two-stage robust optimization approach to address it, thereby promoting energy transactions between microgrids and reducing the operating costs of distribution networks and microgrids. However, centralized algorithms have several notable drawbacks. First, as the system size increases, the computational complexity of the centralized method escalates, leading to longer solution times that are unsuitable for real-time scheduling in large, complex systems. Additionally, centralized methods require substantial information sharing, which not only increases communication costs but also raises concerns about privacy breaches, particularly in scenarios involving multiple stakeholders. Furthermore, since all optimization decisions are made at a central point, any single point of failure could jeopardize the stability and operational efficiency of the entire system. To address these challenges, this paper adopts the automatic transmission control (ATC) algorithm, a distributed approach. The ATC distributed algorithm used in this paper offers strong adaptability, efficient time coordination, reduced communication costs, good robustness, and scalability. ATC optimizes energy scheduling in a distributed manner without the need to share internal information, thereby effectively protecting participant privacy while ensuring an efficient and fair benefit distribution mechanism and highly stable system operation.

This paper proposes a collaborative optimization method for microgrid clusters and the active distribution network (ADN), to improve system operational efficiency and reduce information exchange costs. Unlike traditional microgrid optimization methods, which focus solely on the independent operation of

microgrids, this paper integrates the collaborative optimization of both the microgrid and the distribution network, demonstrating the advantages of microgrid-distribution network coordination. Additionally, this paper employs a distributed algorithm that, compared to traditional centralized algorithms, significantly reduces computational and communication burdens while enhancing the system's scalability and flexibility. Specifically, the ATC algorithm is utilized, which, compared to other distributed algorithms, optimizes decoupling and minimizes information exchange, further improving computational efficiency and optimization performance. The contributions are summarized as follows:

(1) This paper proposes a hierarchical scheduling model and method for the collaborative optimization of microgrid clusters and the ADN, integrating the interaction between both systems. This approach not only improves resource utilization in microgrids and the distribution network, but also enhances the precision of energy scheduling and the overall system's stability. In microgrid modeling, demand response (DR) and multi-energy complementarity are considered, providing a more comprehensive and flexible optimization framework.

(2) This paper proposes a distributed scheduling method based on the ATC algorithm, which significantly reduces the information exchange requirements between the microgrid clusters and the ADN compared to centralized optimization methods. This approach reduces communication costs and computational complexity, providing better adaptability and flexibility, especially in large-scale systems.

(3) Compared with centralized algorithms, the ATC algorithm demonstrates superior feasibility and effectiveness in solving the collaborative optimization problem between microgrid clusters and the ADN. By decomposing the optimization process hierarchically and using coupling variables (such as tie-line power), the ATC method efficiently decouples the systems, reduces internal information exchange, and significantly improves overall computational efficiency, while requiring only limited information sharing between the microgrid clusters and the ADN.

The paper is organized as follows: In Section 2, a model of microgrid clusters' access to ADN is established, including mathematical models for the lower microgrid clusters and upper distribution network. In Section 3, the basic principle of ATC and the solution flow of the collaborative optimization model based on this method are introduced. In Section 4, an example is analyzed using the IEEE-33 node system, and the paper concludes in Section 5.

2 Collaborative Optimization Model of Microgrid Clusters with Distribution Networks

The structure of the ADN system with microgrid clusters is shown in Fig. 1. Microgrid clusters combine the distribution network system, renewable energy (RE) generation devices, various energy coupling and conversion devices, and loads of various energy forms in a certain area. The microgrid clusters can more efficiently absorb the output of renewable energy sources, such as wind and photovoltaic, in the region to meet load demand. When the capacity of microgrid clusters is insufficient or in excess, the microgrid will interact with the superior distribution network to purchase or sell electricity. The microgrid control center rationally schedules the output of each piece of equipment in the microgrid by optimizing scheduling, so that the total operating cost of the microgrid clusters can be minimized while meeting load demand and power balance. Similarly, for the superior distribution network system, it is necessary to meet the active and reactive load demand at each node and balance electric power, thereby achieving the goal of the lowest power purchase cost for the transmission network system. The overall optimization objective can be expressed as shown in Eq. (1).

$$\begin{aligned} &\min f = f_{DN} + f_{MG} \\ &s.t. g(x) \le 0 \\ &\quad h(x) = 0 \end{aligned} \tag{1}$$

where: f_{DN} and f_{MG} are the optimization objectives of the distribution network and microgrid clusters, respectively, $h(x)$ is the equality constraint satisfied by the system, and $g(x)$ is the inequality constraint satisfied by the system.

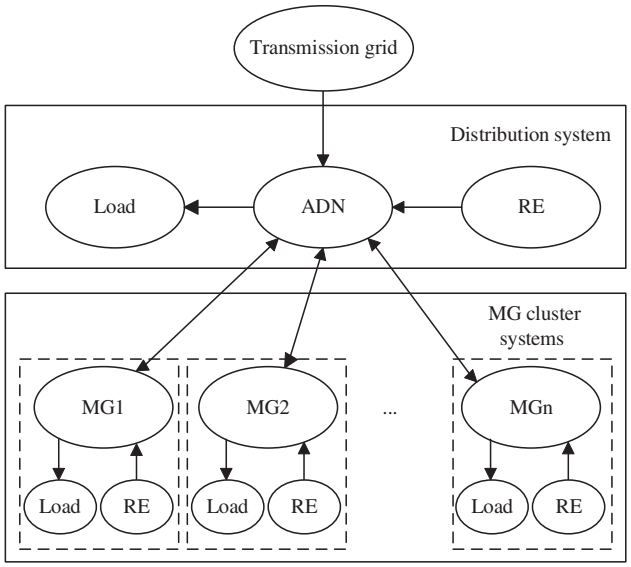

Figure 1: Microgrid clusters are connected to distribution networks

Based on the above, microgrid clusters and the ADN, as a unified interest subject, share an overall objective function while also maintaining their own economic optimization goals [15]. However, due to the coupling effect of the interactive electric power on the tie-line, the two systems not only influence each other in scheduling but also require extensive information exchange, leading to challenges associated with unlimited data sharing. This hierarchical structure and the diverse demands of different stakeholders align well with ATC's solution approach, which supports limited information exchange while reconciling the interests of all parties, reduces the communication burden on the tie-line, and meets the need for constrained data visibility. Therefore, ATC is well-suited for modeling and solving optimal scheduling problems for microgrid clusters integrated into the ADN [16].

2.1 Optimal Scheduling Model of Microgrid Clusters at the Lower Level

In this paper, the microgrid clusters system consists of energy supply equipment such as wind power and photovoltaic, energy coupling and conversion equipment such as power-to-gas, combined heat and power generation and electric heating boilers, energy storage devices such as electricity storage and heat storage, and microgrid clusters with demand response constitute the microgrid clusters. In this system, each microgrid can achieve power balance and optimal scheduling by adjusting purchased and sold electricity on the supply side, demand response on the load side, and charging and discharging of energy storage equipment. The optimization goal of the lower-layer system is to minimize the total operating cost of the entire microgrid cluster, and the constraints are the power balance between the upper and lower limits of each piece of equipment in the system, as well as various forms of energy.

2.1.1 Typical Structure of Microgrid

The structure of an MG is roughly divided into three main parts, namely, the energy supply part, the equipment coupling part, and the user part. A typical microgrid structure is shown in Fig. 2. The green arrow shows the direction of electricity flow, the blue arrow shows the direction of natural gas flow, and the orange arrow shows the direction of heat flow [17,18].

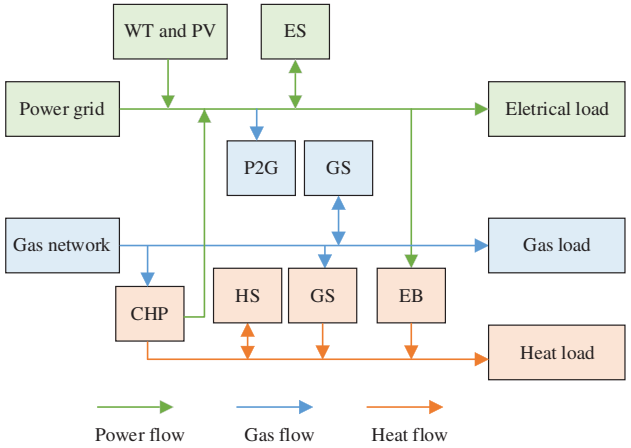

Figure 2: Microgrid structure diagram

2.1.2 Objective

The optimization objective for microgrid clusters is the system's operational cost, as expressed in Eq. (2).

$$f_{\mathrm{MG}} = \min \sum_{i=1}^{n} \sum_{t=1}^{T} \left(C_{\mathrm{buy},i,t} + C_{\mathrm{op},i,t} + C_{\mathrm{ab},i,t} + C_{\mathrm{DR},i,t} \right) \tag{2}$$

where n is the number of microgrid in the system, T is the total scheduling time, $T = 24$ in general, $C_{\mathrm{buy},i,t}$ is the gas purchase cost of the i microgrid in the t period, $C_{\mathrm{op},i,t}$ is the operation and maintenance cost of the i microgrid in the t period, $C_{\mathrm{ab},i,t}$ is the wind power and photovoltaic abandonment cost of the i microgrid in the t period, and $C_{\mathrm{DR},i,t}$ is the DR compensation cost of the i microgrid in the t period.

$$C_{\mathrm{buy},i,t} = p^{\mathrm{G}}_{\mathrm{buy},t} P^{\mathrm{G}}_{\mathrm{buy},i,t} \tag{3}$$

where $p^{\mathrm{E}}_{\mathrm{buy},t}$, $p^{\mathrm{G}}_{\mathrm{buy},t}$, and $p^{\mathrm{E}}_{\mathrm{sell},t}$ are respectively the purchasing price, natural gas price, and selling price, and $P^{\mathrm{E}}_{\mathrm{buy},i,t}$, $P^{\mathrm{G}}_{\mathrm{buy},i,t}$, and $P^{\mathrm{E}}_{\mathrm{sell},i,t}$ are respectively the purchasing power, purchasing gas, and selling power of the i microgrid in period t.

$$C_{\mathrm{op},i,t} = k_{N,i,t} P_{N,i,t} \tag{4}$$

where $k_{N,i,t}$ is the cost coefficient per unit power of the equipment circulating at microgrid i in time period t, and $P_{N,i,t}$ is the power of the equipment circulating at microgrid i in period t.

$$C_{\mathrm{ab},i,t} = \alpha_{\mathrm{w}} \left(P^{\mathrm{W}}_{i,t} - P^{\mathrm{Wc}}_{i,t} \right) + \alpha_{\mathrm{PV}} \left(P^{\mathrm{PV}}_{i,t} - P^{\mathrm{PVc}}_{i,t} \right) \tag{5}$$

where α_{w} and α_{PV} are the unit power penalty coefficients of wind power and photovoltaic abandonment, respectively, $P^{\mathrm{W}}_{i,t}$ and $P^{\mathrm{PV}}_{i,t}$ are the output of wind power and photovoltaic, respectively, and $P^{\mathrm{Wc}}_{i,t}$ and $P^{\mathrm{PVc}}_{i,t}$ are the wind power and photovoltaic absorbed by the i microgrid within the t period, respectively.

$$C_{\mathrm{DR},i,t} = C_{i,t}^{\mathrm{shift}} + C_{i,t}^{\mathrm{tran}} + C_{i,t}^{\mathrm{cut}} \tag{6}$$

where $C_{i,t}^{\mathrm{shift}}$, $C_{i,t}^{\mathrm{tran}}$, and $C_{i,t}^{\mathrm{cut}}$ represent the compensation costs of shiftable load, transferable load, and reducible load in each microgrid, respectively.

2.1.3 Constraint

The constraints of microgrid clusters mainly include power balance constraints across various energy forms, upper and lower limit constraints on interactive power between the microgrid and the liaison line of the upper energy supply system, and output and power balance constraints for each device within the microgrid.

(1) Constraints on interactive power

$$\begin{cases} P_{i,t}^{\mathrm{grid}} = P_{i,t}^{\mathrm{pcc}} \\ P_{\min}^{\mathrm{grid}} \le P_{i,t}^{\mathrm{grid}} \le P_{\max}^{\mathrm{grid}} \end{cases} \tag{7}$$

$$\begin{cases} G_{i,t}^{\mathrm{grid}} = G_{i,t}^{\mathrm{pcc}} \\ G_{\min}^{\mathrm{grid}} \le G_{i,t}^{\mathrm{grid}} \le G_{\max}^{\mathrm{grid}} \end{cases} \tag{8}$$

where $P_{i,t}^{\mathrm{pcc}}$ and $G_{i,t}^{\mathrm{pcc}}$ are the electric power and gas power that the i microgrid interacts with the superior distribution network and the gas supply pipeline during the period t, $P_{\min}^{\mathrm{grid}}$ and $P_{\max}^{\mathrm{grid}}$ are the lower limit and upper limit of the interactive electric power between microgrid and the distribution network liaison line, and $G_{\min}^{\mathrm{grid}}$ and $G_{\max}^{\mathrm{grid}}$ are the lower limit and upper limit of the interactive natural gas power between the microgrid and the natural gas supply pipeline, respectively.

(2) Power balance constraint

$$\begin{cases} P_{i,t}^{\mathrm{grid}} + P_{i,t}^{\mathrm{ren}} + P_{i,t}^{\mathrm{ES}} + P_{i,t}^{\mathrm{dev}} + P_{i,t}^{\mathrm{load}} = 0 \\ G_{i,t}^{\mathrm{grid}} + G_{i,t}^{\mathrm{ES}} + G_{i,t}^{\mathrm{dev}} + G_{i,t}^{\mathrm{load}} = 0 \\ H_{i,t}^{\mathrm{ES}} + H_{i,t}^{\mathrm{dev}} + H_{i,t}^{\mathrm{load}} = 0 \end{cases} \tag{9}$$

where $P_{i,t}^{\mathrm{ren}}$ is the output of renewable energy, $P_{i,t}^{\mathrm{ES}}$, $G_{i,t}^{\mathrm{ES}}$, and $H_{i,t}^{\mathrm{ES}}$ are the operating power of the electricity storage, gas storage and heat storage device, respectively, $P_{i,t}^{\mathrm{dev}}$, $G_{i,t}^{\mathrm{dev}}$, and $H_{i,t}^{\mathrm{dev}}$ are the output power of the energy coupling and conversion equipment in the microgrid, $P_{i,t}^{\mathrm{load}}$, $G_{i,t}^{\mathrm{load}}$, and $H_{i,t}^{\mathrm{load}}$ are the electricity, gas, and heat load, respectively.

(3) Mathematical models and constraints of microgrid devices

Using the typical structure in Fig. 2 as an example, the mathematical models and constraints for each device in the microgrid are established.

(1) Wind Power and Photovoltaic

$$\begin{cases} 0 \le P_t^{\mathrm{PVc}} \le P_t^{\mathrm{PV}} \\ 0 \le P_t^{\mathrm{Wc}} \le P_t^{\mathrm{W}} \end{cases} \tag{10}$$

(2) Gas Boiler (GB)

$$\begin{cases} H_t^{\mathrm{GB}} = \eta^{\mathrm{GB}} G_t^{\mathrm{GB}} \\ H_{\min}^{\mathrm{GB}} \le H_t^{\mathrm{GB}} \le H_{\max}^{\mathrm{GB}} \end{cases} \tag{11}$$

where H_t^{GB} is the thermal power of the gas boiler at time t; η^{GB} is the energy conversion efficiency of the gas-fired boiler; G_t^{GB} is the gas power consumed by the gas boiler at time t; H_{min}^{GB} and H_{max}^{GB} are the lower limit and upper limit of the thermal power of the gas boiler, respectively.

(3) Electric Boiler (EB)

$$\begin{cases} H_t^{EB} = \eta^{EB} P_t^{EB} \\ H_{min}^{EB} \le H_t^{EB} \le H_{max}^{EB} \end{cases} \tag{12}$$

where H_t^{EB} and P_t^{EB} are respectively the heat generation power and power consumption power of EB at time t; η^{EB} is the electric heating conversion efficiency.

(4) Power-to-Gas (P2G)

$$\begin{cases} G_t^{P2G} = \eta^{P2G} P_t^{P2G} \\ 0 \le G_t^{P2G} \le G_{max}^{P2G} \end{cases} \tag{13}$$

where G_t^{P2G} and P_t^{P2G} are respectively the gas power and electric power consumed by the P2G device during the t period; η^{P2G} is the conversion efficiency; G_{max}^{P2G} is the maximum atmospheric power of natural gas generated by P2G.

(5) Combined Heat and Power (CHP)

$$\begin{cases} P_{min}^{CHP} \le P_t^{CHP} \le P_{max}^{CHP} \\ P_t^{CHP} = \eta_P^{CHP} G_t^{CHP} \\ H_t^{CHP} = \eta_H^{CHP} G_t^{CHP} \\ R_{down}^{CHP} \le P_t^{CHP} - P_{t-1}^{CHP} \le R_{up}^{CHP} \end{cases} \tag{14}$$

where P_{min}^{CHP} and P_{max}^{CHP} are respectively the maximum and minimum power generation under CHP pure condensation condition; P_t^{CHP}, G_t^{CHP}, and H_t^{CHP} are the generation power, natural gas consumption power, and heat production power of CHP at time t, respectively. η_P^{CHP} and η_H^{CHP} are the efficiency of CHP burning natural gas to convert into electric energy and heat energy, respectively. R_{down}^{CHP} and R_{up}^{CHP} are the downhill power and uphill power of CHP, respectively.

(6) Energy Storing Device

The model established in this paper includes energy storage (ES) devices for electricity, heat, and gas. The operating principles and energy conversion relationships of these three types of energy storage devices are similar, so a unified model can be used to describe all three. For example, the operational constraints of electrical energy storage can be expressed as shown in Eq. (15).

$$\begin{cases} W_t^{ES} = W_{t-1}^{ES} + \eta^{ESc} P_t^{ESc} \Delta t - \dfrac{P_t^{ESd} \Delta t}{\eta^{ESd}} \\ W_{min}^{ES} \le W_t^{ES} \le W_{max}^{ES} \\ 0 \le P_t^{ESc} \le A_t^c P_{max}^{ESc} \\ 0 \le P_t^{ESd} \le A_t^d P_{max}^{ESd} \\ A_t^c + A_t^d \le 1 \\ W_0^{ES} = W_T^{ES} \end{cases} \tag{15}$$

where W_t^{ES} is the stored electricity of the electric energy storage at time t; P_t^{ESc} and P_t^{ESd} are the charging power of the electric energy storage and discharging power of the electric energy storage at time t, respectively. η^{ESc} and η^{ESd} are the charging efficiency and discharge efficiency, respectively. Δt is

the time interval; $W_{\min}^{ES}$ and $W_{\max}^{ES}$ are the minimum and maximum capacity of electric energy storage, respectively. $P_{\max}^{ESc}$ and $P_{\max}^{ESd}$ are the charging power and discharge power of the electric energy storage, respectively. A_t^c and A_t^d are charge and discharge marks of the electric energy storage, respectively, and are 0–1 variables. $A_t^c = 1$ indicates that the electric energy storage works in the charging state, and $A_t^d = 1$ indicates that the electric energy storage works in the discharge state. W_0^{ES} and W_T^{ES} represent the amount of electricity stored in the initial and final stages of the scheduling, respectively.

2.2 Optimal Power Flow Model of the Upper Distribution Network

2.2.1 Objective

The optimal power flow calculation model for the upper distribution network aims to minimize power purchases from the main network.

$$f_{DN} = \min \mu_1 P_g \tag{16}$$

where P_g is the power purchased by the distribution network from the main network, and μ_1 is the price of purchasing electricity from the main network.

2.2.2 Constraint

(1) Liaison line power constraints

$$P_{\min}^{pcc} \le P_{i,t}^{pcc} \le P_{\max}^{pcc} \tag{17}$$

where $P_{\min}^{pcc}$ and $P_{\max}^{pcc}$ represent the minimum and maximum circulating electric power of the distribution network and microgrid liaison line, respectively.

(2) System security constraint

To ensure the safe and stable operation of the distribution network system, the voltage at each node and the current flowing through each line should be within certain ranges, as shown in Eqs. (18) and (19).

$$V_{\min}^2 \le V_{i,t}^2 \le V_{\max}^2 \tag{18}$$

$$I_{\min}^2 \le i_{ij,t}^2 \le I_{\max}^2 \tag{19}$$

where $V_{\min}$ and $V_{\max}$ are the minimum and maximum value of node voltage, respectively; $V_{i,t}$ is the voltage of node i at time t; $I_{\min}$ and $I_{\max}$ are the minimum and maximum current allowed to flow by branch current, respectively; $i_{ij,t}$ is the current flowing by branch ij at time t.

(3) Distflow power flow constraint of the distribution network

$$P_{ij,t} - r_{ij} I_{ij,t}^2 + P_{i,n,t}^{in} = \sum_{u \in \pi(j)} P_{ju,t} + P_{j,t}^L \tag{20}$$

$$Q_{ij,t} - x_{ij} I_{ij,t}^2 + Q_{i,n,t}^{in} = \sum_{u \in \pi(j)} Q_{ju,t} + Q_{j,t}^L \tag{21}$$

$$V_{j,t}^2 = V_{i,t}^2 - 2\left(r_{ij} P_{ij,t} + x_{ij} Q_{ij,t}\right) + \left(r_{ij}^2 + x_{ij}^2\right) I_{ij,t}^2 \tag{22}$$

$$I_{ij,t}^2 = \frac{P_{ij,t}^2 + Q_{ij,t}^2}{V_i^2} \tag{23}$$

where $P_{ij,t}$ and $Q_{ij,t}$ are the active and reactive power at the beginning of branch ij at time t, $P_{i,n,t}^{in}$ and $Q_{i,n,t}^{in}$ are the active and reactive power injected by the microgrid into the distribution network at time t, r_{ij} and x_{ij} are the resistance and reactance of branch ij, respectively, u is the child node, $\pi(j)$

is the child node set of the bus where the node is located, $P_{ju,t}$ and $Q_{ju,t}$ are the active and reactive power transferred to the child node, respectively. $P^L_{j,t}$ and $Q^L_{j,t}$ are the active and reactive loads of node j, respectively.

In order to find the global optimal solution, the power flow equation is relaxed, and the nonlinear optimal power flow model is transformed into a second-order cone model, and Eq. (23) is transformed into Eq. (24).

(4) Reactive power compensation device constraints

For each reactive power compensation equipment, in each period of time, the compensated reactive power should be within a certain range, not exceeding the maximum reactive power capacity of its output and not less than the minimum capacity.

$$Q^n_{\min} \le Q^n_{i,t} \le Q^n_{\max} \tag{24}$$

where n is the type of reactive power compensation equipment, including a capacitor bank and a static reactive power compensator, and $Q^n_{\min}$ and $Q^n_{\max}$ are respectively the minimum reactive power and the maximum reactive power that reactive power compensation equipment n can compensate in the t period.

3 Collaborative Optimization Model Based on ATC

3.1 The Basic Principle and Decoupling Control of ATC

ATC is a method proposed in the Journal of Mechanical Design in 2003 to solve multi-level optimization problems in complex systems, and its principle is shown in Fig. 3 [19]. As shown in Fig. 3, the basic principle of ATC is to propagate the target from the main system to each subsystem, gradually optimize different objective functions by layers, and have the optimization model at all levels respond in turn, with feedback from bottom to top. Each system is solved independently. After optimizing the upper system, the coupling variables are passed to the lower subsystem, which takes them as its goal. On the premise of meeting its own constraints and conditions, the module component is designed to optimize its own problems, and a penalty term is introduced into the analysis module component to ensure the optimization value remains close to the target. Similarly, the superior system will also perform this process, alternating between optimizations until the convergence condition is met. In this way, the priority relationship between the goals is clearly defined, and the problem's complexity is effectively reduced.

In the traditional centralized optimization algorithm, the optimal power flow model of the distribution network and the economic optimal scheduling model of microgrid clusters are solved simultaneously. In this process, information is shared between the upper distribution network system and the lower microgrid clusters, and information transfer and coupling control are carried out between the distribution network and the microgrid clusters via the liaison line's interactive power. They can not be solved independently. The method shown in Fig. 4 can be used to decouple the upper distribution network system from the lower microgrid clusters.

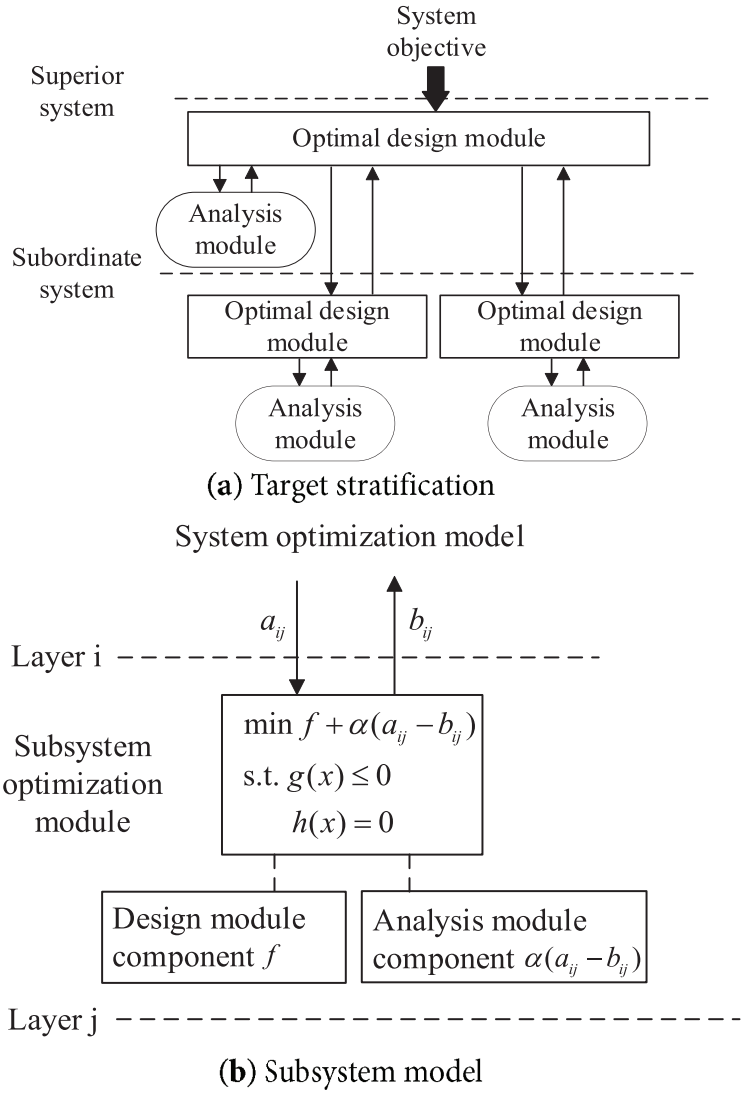

Figure 3: Theory of ATC

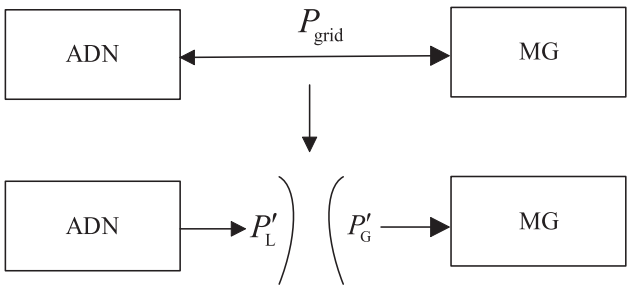

Figure 4: Decoupling control of the distribution network and microgrid clusters

3.2 The Solution Flow of ATC

The ADN is the upper system of the ATC algorithm, and the microgrid clusters are the lower system. The ATC is used to solve the optimal scheduling model in this paper. The solving process is as follows [20]:

(1) Input the parameters of the distribution network, set the initial value of interactive power P'_{G} and P'_{L} and the initial value of the multiplier of the penalty function, and set the number of iterations to 1.

(2) According to the equipment of each microgrid, the optimal scheduling solution model is established. At the same time, the initial coupling variable is passed to the microgrid clusters as the default initial value. At this time, the objective function of the microgrid clusters is modified as follows:

$$\min\left[f_{\mathrm{MG}}+\sum_{t=1}^{T}\alpha_{k,t}\left(P'_{\mathrm{G}}-P'_{L}\right)+\sum_{t=1}^{T}\beta_{k,t}\left(P'_{\mathrm{G}}-P'_{L}\right)^{2}\right] \tag{25}$$

where f_{MG} is the original objective function of the lower system, and $\alpha_{k,t}$ and $\beta_{k,t}$ are the first and second coefficients of the Lagrange penalty function after the KTH iteration, respectively.
According to the new objective function, the coupling variable P'_{G} with power properties is obtained by optimizing the solution.

(3) After the three groups of microgrid are solved in parallel, the coupling variable P'_{G} obtained by each group is passed to the upper distribution network system. Meanwhile, the objective function of the distribution network system is modified in a manner similar to Eq. (25). While the distribution network is optimized, the coupling variable of new power supply properties is passed to the microgrid clusters.

(4) Check whether the result meets the convergence condition. If so, the iteration ends and the optimal scheduling result is output; otherwise, the penalty function multiplier is updated, and the step 2 is repeated until the convergence condition is met.

The Euclidean distance between the interactive power of the power supply and the interactive power of the load is calculated according to Eqs. (26) and (27), so that the two are close to each other numerically, and whether the convergence condition is met is judged.

$$\left|P'_{G}-P'_{L}\right|\leq\varepsilon_{1} \tag{26}$$

$$\left|\frac{\left(f_{\mathrm{DN}}^{k}+f_{\mathrm{MG}}^{k}\right)-\left(f_{\mathrm{DN}}^{k-1}+f_{\mathrm{MG}}^{k-1}\right)}{f_{\mathrm{DN}}^{k}+f_{\mathrm{MG}}^{k}}\right|\leq\varepsilon_{2} \tag{27}$$

where, ε_1 and ε_2 are error precision. Eq. (26) indicates that the difference between the interactive power P'_G of the power supply property and the interactive power P'_L of the load property should meet the accuracy requirements; Eq. (27) indicates that the total cost of the superior distribution network reaches an optimal level.

If the convergence condition is met, the optimal scheduling result is output; if the convergence condition is not met, the new Lagrange multiplier is calculated according to Eqs. (28) and (29), and the iteration is repeated until the convergence condition is met.

$$\alpha_{k+1,t}=\alpha_{k,t}+2\beta_{k,t}^{2}\left|P_{G}^{'}-P_{L}^{'}\right| \tag{28}$$

$$\beta_{k+1,t}=\gamma\beta_{k,t} \tag{29}$$

In the equations, γ is the coefficient, and the number between 2 and 3 is generally taken.

The specific solution process is shown in Fig. 5.

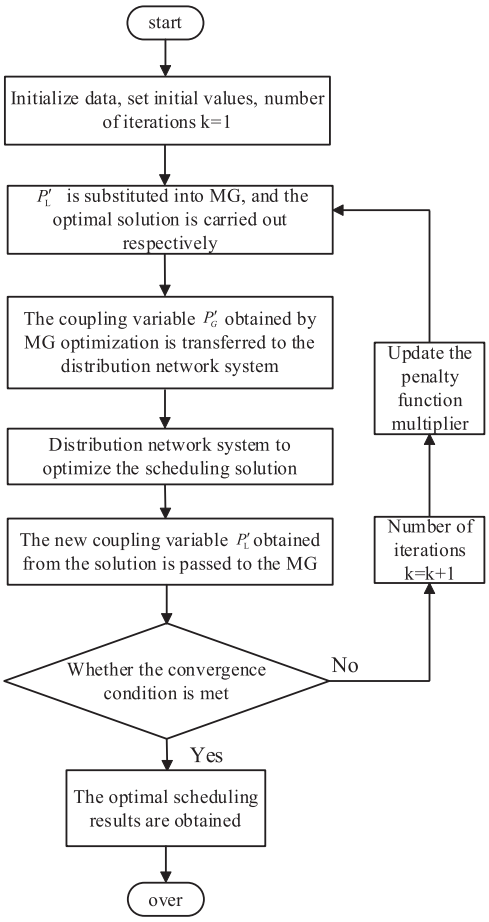

Figure 5: The solution flow of ATC

4 Case Study

4.1 Explanation of Basic Data and Example

The calculation example in this section selects the IEEE33-nodes standard calculation example, three microgrids are connected to node 10, node 23 and node 28, respectively, the wind farm is connected to node 17 and node 33, respectively, the reactive power compensation device is connected to node 7, node 15 and node 31, respectively, and power storage device is connected to node 15 and node 33, respectively. To maintain node voltage stability, three groups of −100~300 kvar static var compensators (SVCS) and two groups of 100 kvar capacity switching capacitors are installed in the system. Specific structure is shown in Fig. 6. The power base is 1 megawatt, and the voltage base is 12.66 kilovolts.

Parameters for coupling and storage devices, time-of-use electricity price, gas prices and demand response parameters in the microgrid are shown in Ref. [21].

As shown in Fig. 6, two wind turbines are connected to the distribution network side, and wind power and photovoltaic power generation, also connected to the microgrid are combined into a new energy output. A representative typical case extracted from realistic data is shown in Fig. 7. It should be stated that the proposed model and solution algorithm are general and applicable to a wide range of renewable generation profiles.

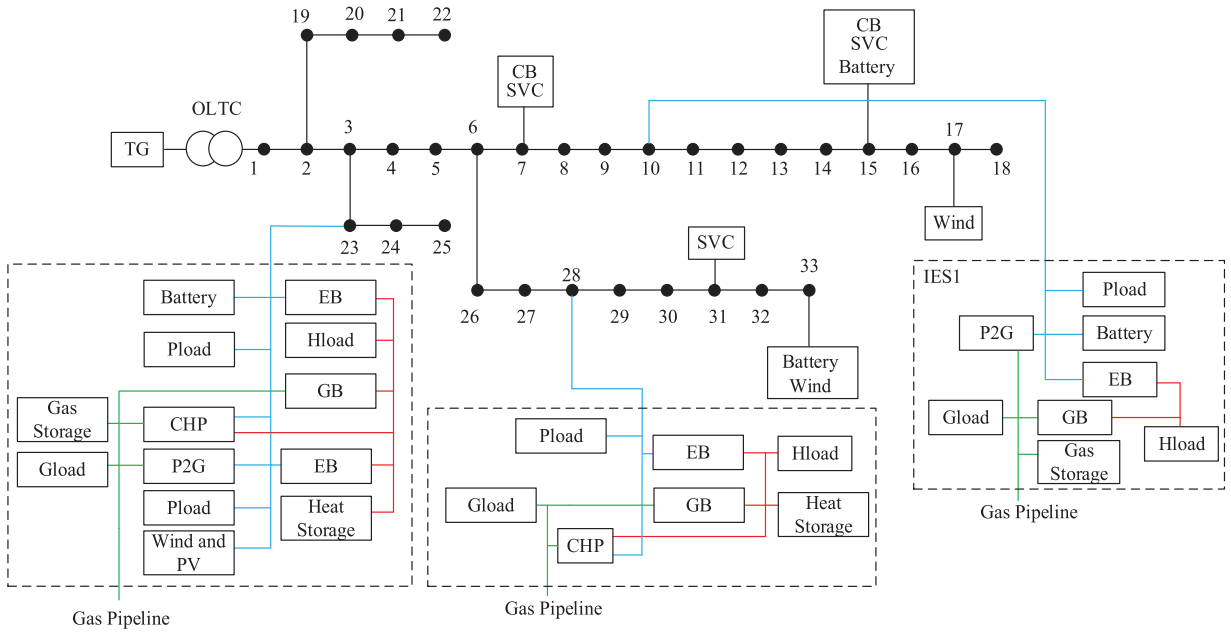

Figure 6: Network structure of the IEEE-33 nodes distribution system

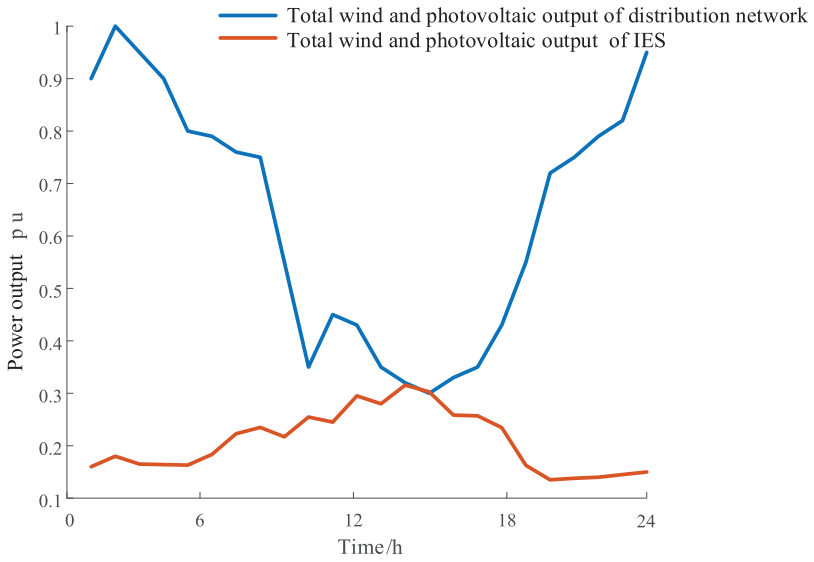

Figure 7: Renewable energy output power

4.2 Optimal Scheduling Results Based on ATC

4.2.1 Iterative Convergence Case

Based on the established collaborative optimization model, ATC is used for an iterative optimization with convergence accuracy is set to 10^{-3}. The iteration process is shown in Fig. 8. After 7 iterations, convergence is achieved, and the total cost is about 41,185.3 yuan. The exchange rate from Chinese yuan to US dollars is fixed at 0.1839 per yuan.

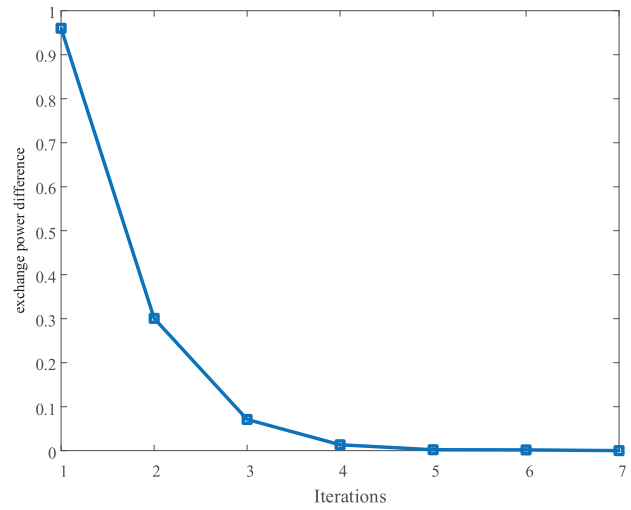

(**a**) Error

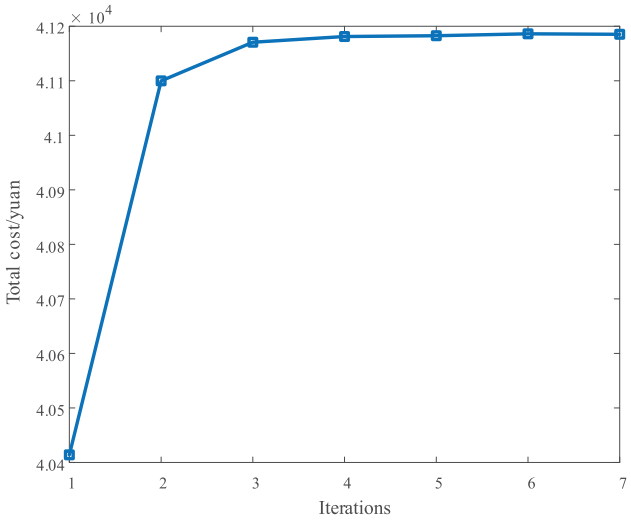

(**b**) Total cost

Figure 8: Iterative process

Taking the interactive power of the distribution network and the MG group at the 10th and 21st moments as examples, their power-convergence process is shown in Fig. 9. The interactive power between the upper distribution network and the microgrid clusters gradually converge, and eventually the interactive power between the upper distribution network and the lower microgrid clusters reaches the same level, and the economy of two groups reach an optimal level.

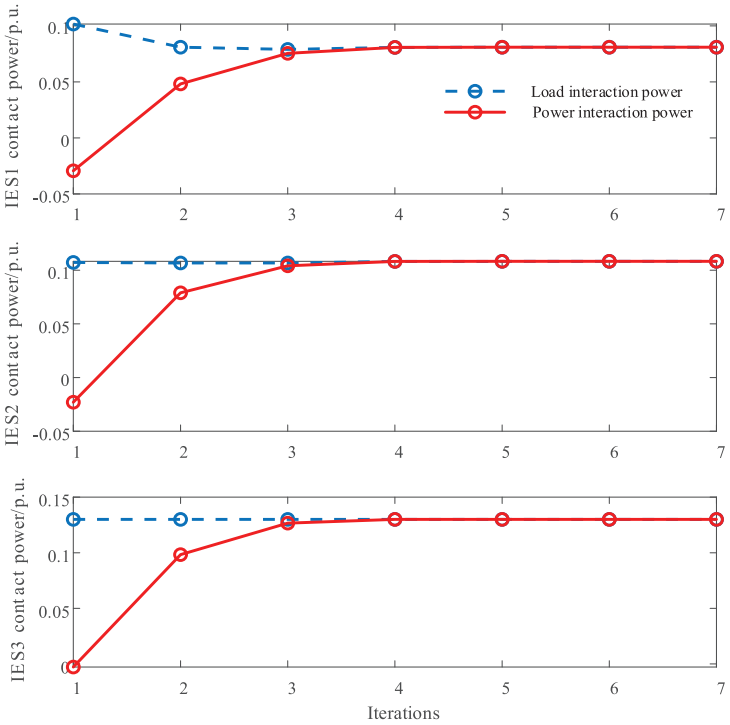

(**a**) The tenth moment

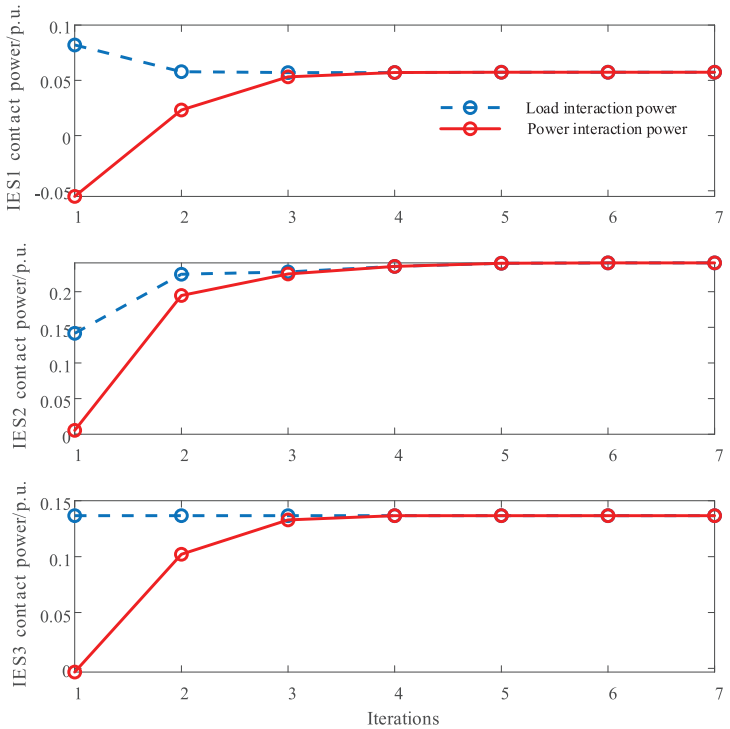

(**b**) The 21st moment

Figure 9: The convergent process of interactive power

4.2.2 Optimal Scheduling Result

The results of day-ahead scheduling are shown in Figs. 10–15, where the electrical power of three microgrids is shown in Figs. 10–12. The interactive power is the power flowing through the connection line between the distribution network and microgrid; positive power is the power flowing through the connection line, that is, the microgrid buys electricity to the distribution line; the negative power is the power flowing through the connection line, that is, the microgrid sells electricity to the distribution network; when the circulating power on the connection line is 0, it means that there is no power purchasing and selling relationship between microgrid and the distribution network.

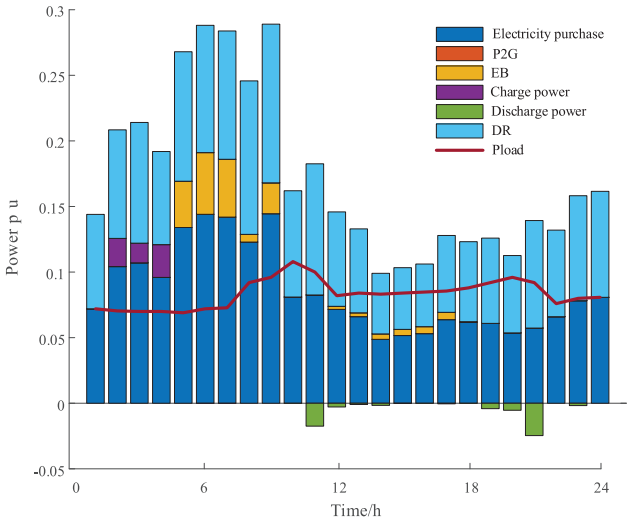

Figure 10: Electrical power of microgrid 1

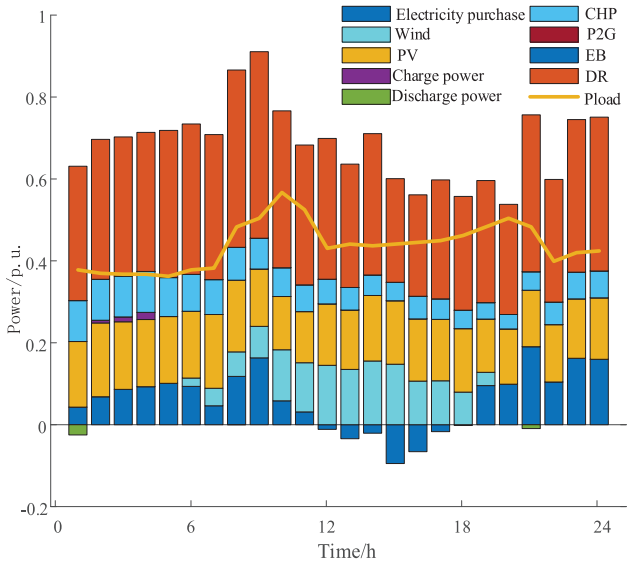

Figure 11: Electrical power of microgrid 2

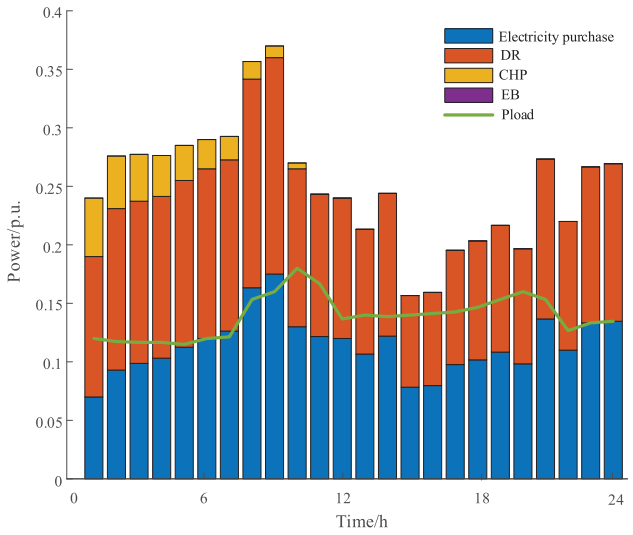

Figure 12: Electrical power of microgrid 3

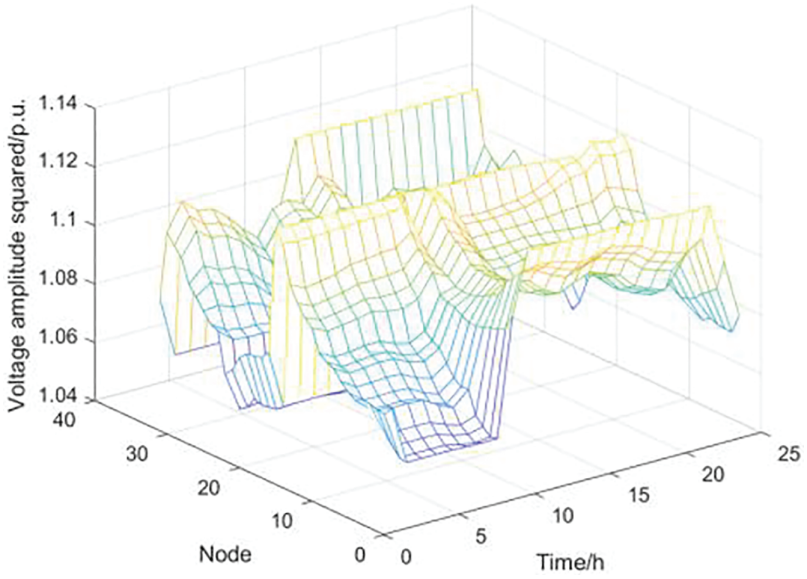

Figure 13: Square of voltage amplitude

In microgrid 1 and microgrid 3, because there is no access to wind power and photovoltaic power, their power consumption mainly depends on the purchase of power from the superior distribution network, while microgrid 2 has wind power and photovoltaic power generation, so it can supply electricity by itself, and the dependence on the superior distribution system is relatively small. At time 0–7, the electricity price is the valley-hour price; at the same time, demand response occurs on the load side, and part of the peak-load electricity is transferred to the valley-hour and normal price periods. At this time, the microgrid's battery charges and stores electric energy to supply the system's load during the peak price period. Therefore, microgrid 3's power consumption primarily depends on power purchased from the higher power grid. During the peak period of electricity prices, the system will transfer more transferable loads and shifting loads to the peak period, and also reduce peak electricity price loads.

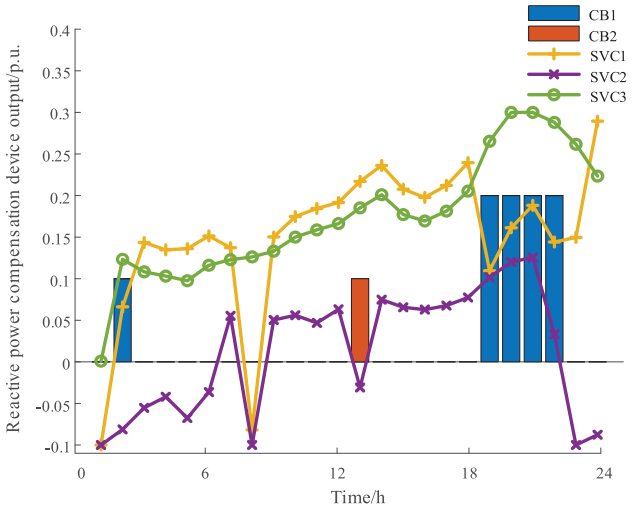

Figure 14: Reactive power compensation device diagram

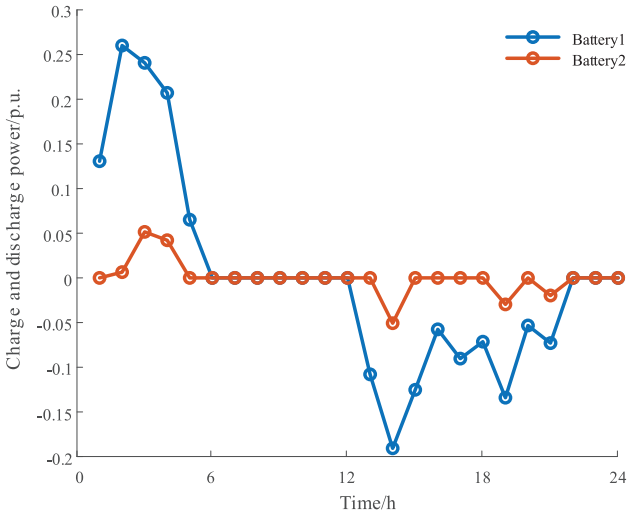

Figure 15: Battery charging and discharging power

During 10–15 h at noon and 19–22 h at night, when electricity prices are at peak, demand response reduces load consumption, and the battery is discharged during these periods, avoiding the microgrid from buying more expensive power. At the same time, due to the output of microgrid 2 electricity and photovoltaic power and the power emitted by the CHP device, the microgrid 2 power supply and the CHP power supply are reduced. This increases the system's power surplus, allowing the microgrid to sell power to the distribution network.

Figs. 13–16 show the scheduling status of the upper-layer distribution network system. Based on the 12.66 kV distribution network, the voltage fluctuation range is ±7%, meaning the squared voltage magnitude should be between 0.8649 and 1.1449 p.u. Additionally, due to the overgeneration from distributed resources, the voltage at some nodes may be at a higher level, but it remains within the safe range. The square of voltage magnitudes is shown in Fig. 13, with the square of the voltage amplitude at each node maintained between 1.05 and 1.12 p.u. which is below the safety limit of 1.1449 p.u. and thus meets the voltage safety requirements. As can be seen from Fig. 15, the compensation of the reactive power compensation device is low at 0–7

moments, and the square of the voltage amplitude of some nodes in the system is 1.05–1.059 p.u. Within the range, the reactive power output is higher during 10–20 h, and the node voltage during this period also increases correspondingly. Fig. 16 shows the operating state of the energy storage device in the distribution network. The battery charges when the electricity price is low and discharges when the electricity price is high to meet the power demand of the system's electrical load.

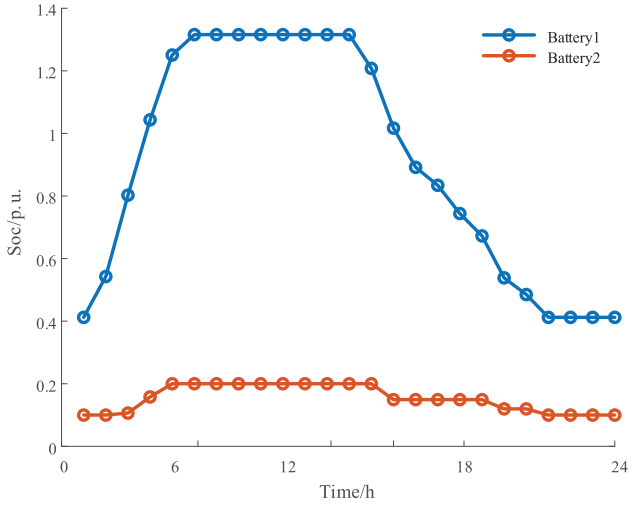

Figure 16: Battery SOC status diagram

4.3 Comparison with Centralized Algorithms

For coordinating distribution systems with multi-energy microgrids, a centralized optimization algorithm is a representative mainstream solution adopted in the existing literature and practice. For the microgrid clusters consisting of 3 microgrids connected to the superior distribution network built in this paper, ATC and the centralized algorithm are compared.

For the centralized algorithm, we used CPLEX as the solver, with relative error tolerance set to 0.0001%, the integer programming error tolerance set to 0.0001%, and the maximum solving time of 3600 s, ensuring that the calculation completes within 1 h to obtain the optimal solution. Since the centralized algorithm does not rely on an iterative process, the stopping criterion is automatically determined by the solver's internal mechanism. The algorithm terminates when the solver finds the optimal solution within the specified time.

For the ATC algorithm, we also used CPLEX, with the relative error tolerance set to 0.001%, the integer programming error tolerance set to 0.0001%, the maximum solving time set to 3600 s, and the maximum node search limit set to 10,000. Regarding the convergence criterion, the ATC algorithm's convergence tolerance is set to 0.1%, meaning that when the change in the objective function between two consecutive iterations is smaller than this value, the algorithm is considered to have converged. The maximum iteration count is set to 100, and if convergence is not achieved within 100 iterations, the algorithm will stop automatically.

The results are shown in Table 1. Compared with the centralized algorithm, the total cost of the ATC adopted in this paper is 41,185.3 yuan, whereas the centralized algorithm's total cost is 41,092.1 yuan. Compared with the centralized algorithm, the deviation in the economic indicators calculated by ATC is about 0.23%, and the results are generally close. In terms of calculation time, the ATC algorithm takes 18.3 s, while the centralized algorithm takes 14.5 s. In terms of time, the centralized algorithm is relatively fast, but the gap is not large.

Table 1: Comparison of ATC and centralized algorithm

Calculation method	Iterations	Calculation time/s	Cost/yuan
ATC	7	18.3	41,185.3
Centralized algorithm	1	14.5	41,092.1

During the iterative process of ATC, the distribution network and the MG only need to exchange information on the interactive electrical power to complete optimization. This significantly reduces the data reporting between the distribution network and the MG. Therefore, as the number of MG connected to the power grid and entering the power market increases, the optimization method based on ATC between the distribution network and the MG will be more adaptable.

The comparison between the power purchased by the distribution network from the main network based on ATC and the centralized algorithm is shown in Fig. 17. As can be seen from the figure, the power purchased by the distribution network from the main network under the two methods basically coincides, and there is a certain deviation between the two methods, but compared with the overall value, the deviation is negligible, so it can be proved that ATC has global convergence. Effectiveness of two-layer optimization in microgrid clusters' access distribution network.

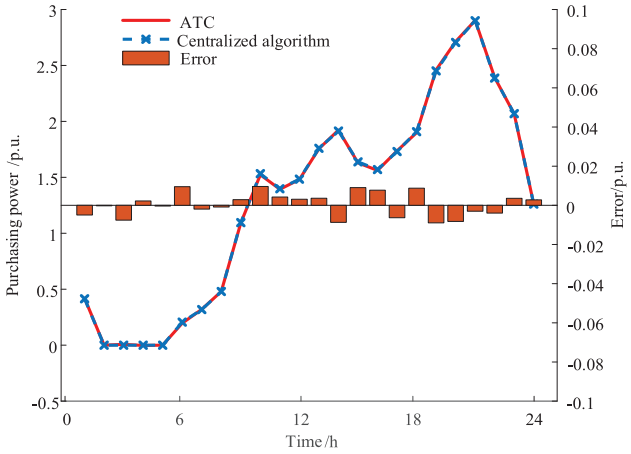

Figure 17: Results comparison of ATC and a centralized manner

4.4 The Performance of ATC

4.4.1 The Influence of Convergence Accuracy

In theory, when the convergence accuracy decreases, the result calculated by ATC will be closer to the centralized algorithm. By changing the convergence accuracy, the objective function value obtained is consistent with the optimization pair of the centralized algorithm, as shown in Table 2.

As shown in Table 2, with the increasing convergence accuracy, the number of iterations gradually increases, and the optimized results are close to the objective function value of centralized calculation. When the convergence accuracy is 10^{-2}, the deviation percentage is only about 0.36%, and the calculation time is fast. In engineering practice, when the accuracy is not particularly high, ATC is very suitable for this accuracy. When the convergence accuracy is 10^{-5}, the deviation between the objective function value calculated by ATC and the objective function value obtained by centralized optimization is less than 0.1%, which is almost

the same. However, due to the increase in the number of iterations, the calculation time is greatly increased, which does not meet the practical calculation requirements of engineering.

Table 2: ATC objective function values with different convergence accuracy

Convergence precision	10^{-2}	10^{-3}	10^{-4}	10^{-5}
The number of times convergence is reached	5	7	10	12
Objective function value/yuan	41,239.6	41,185.3	41,147.5	41,114.6
The difference from the centralized algorithm/yuan	147.5	93.2	55.4	22.5
Percentage difference	0.36%	0.23%	0.13%	0.054%

4.4.2 The Influence of System Scale

To verify the performance of ATC, different numbers of MG were connected in the IEEE-33 node system, and a comparative study was conducted using both ATC and centralized algorithms. In this study, the convergence accuracy of ATC was set at 10^{-3}. The comparison results are shown in Table 3.

Table 3: Objective function values for different MG quantities

The number of MG		3	6	9	12
Total cost/yuan	Centralized algorithms	41,092.1	58,302.3	75,561.2	92,872.6
	ATC	41,185.3	58,448.4	75,750.6	93,105.4
Computation time/s	Centralized algorithms	14.5	25.6	39.5	59.3
	ATC	18.3	27.2	34.8	42.6
The percentage of deviations from the centralized model		0.23%	0.25%	0.27%	0.28%

From Table 3, it can be seen that when only 3 MG are connected to the distribution network, the amount of information in the system is relatively small, and the problem scale is also small. In terms of solving speed, the centralized algorithm has certain advantages. When the number of MG connected to the distribution network is greater, the amount of information to be processed significantly increases, and the problem scale becomes very large. This indicates that the algorithm places a greater burden on itself in large-scale scenarios. In contrast, the speed advantage of ATC in handling such problems gradually becomes evident. As the number of main entities in the lower-level MG increases, the scale effect of ATC becomes more pronounced, and its computing speed and efficiency improve significantly.

From the optimization results, the deviation between the ATC and the centralized optimization scheduling results remained within a relatively small range, indicating that ATC has high reliability in handling large-scale MG access to the distribution network system.

4.4.3 The Influence of the Initial Value

This paper randomly selected 20 different initial values to study the influence of initial values on the objective function. The results are shown in Fig. 18.

As shown in Fig. 18, different initial values have a certain impact on the objective function, but the fluctuation range of the corresponding objective function values is relatively small, remaining around 41,200 yuan overall. The maximum value and minimum value differ by approximately 70 yuan. This indicates that,

even with different initial values, ATC can still ensure the final solution is within the optimal range. It shows that ATC is less affected by initial values, reducing the problem of performance decline caused by improper initial value settings.

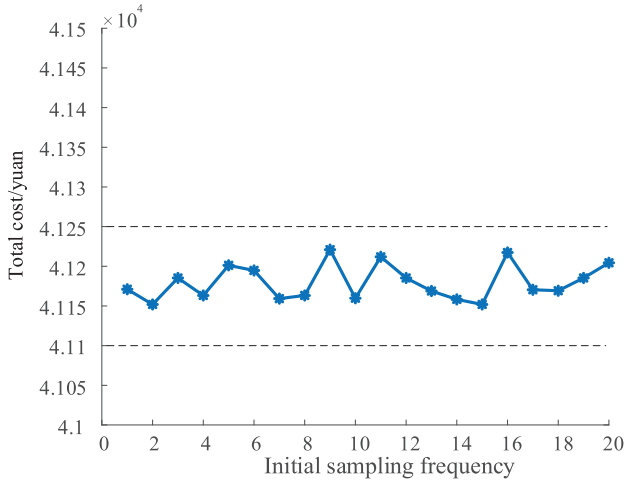

Figure 18: The influence of the initial value on the objective

5 Conclusion

In this paper, a two-layer collaborative optimization model for ADNs and microgrid clusters based on the ATC method is proposed. The upper-layer optimization model aims to minimize power purchases from the distribution network to the main network while minimizing network losses. The lower-layer optimization model, which represents the microgrid clusters, incorporates electrical load demand response and thermal load considerations, aiming to minimize the total operating cost of the microgrid clusters. The Yalmip platform in MATLAB is used to build the IEEE-33 node simulation model, and the CPLEX solver is employed for iterative solution. By comparing the proposed method with a centralized algorithm, the effectiveness and correctness of the established collaborative optimization model and the iterative solution based on ATC are validated. Additionally, the ATC approach significantly reduces the amount of information transmission, which is crucial for privacy and efficiency in distributed systems.

However, the current study assumes a single-phase balanced model and relies on a deterministic optimization approach, which does not account for three-phase unbalanced conditions or the stochastic nature of renewable generation. In future research, we plan to address several key areas, including incorporating three-phase unbalanced constraints into the distribution network optimization model to better represent real-world conditions, developing a coordinated multi-time-scale optimization framework that integrates day-ahead and intra-day decision-making, and conducting more comprehensive comparative studies against alternative solution methods such as the Karush-Kuhn-Tucker (KKT)-condition-based method, bisection search, and particle swarm optimization to thoroughly assess and validate the proposed approach's overall performance. To address these challenges, we emphasize that the framework is designed to be scalable, ensuring its applicability to larger and more complex systems.

Acknowledgement: Not applicable.

Funding Statement: This research was funded by a technology project from the State Grid Corporation of China under grant number JC2024122.

Author Contributions: Conceptualization, Qianfeng Wu; methodology, Rongqiang Li; software, Dabo Xie and Wenhua Ni; validation, Junjie Zhou; formal analysis, Xuantong Lu; investigation, Chengying Ma; resources, Yang Li; data curation, Rongqiang Li; writing—original draft preparation, Yang Li and Rongqiang Li; writing—review and editing, Wenhua Ni and Rongqiang Li; visualization, Wenhua Ni; supervision, Yang Li; project administration, Yang Li. All authors reviewed the results and approved the final version of the manuscript.

Availability of Data and Materials: The data that support the findings of this study are available from the corresponding authors upon reasonable request.

Ethics Approval: Not applicable.

Conflicts of Interest: The authors declare no conflicts of interest to report regarding the present study.

Abbreviation

AND	Active distribution network
ATC	Automatic transmission control
DR	Demand response
RE	Renewable energy
MG	Microgrid
GB	Gas boiler
EB	Electric boiler
P2G	Power-to-gas
CHP	Combined heat and power
ES	Energy storage
SVCS	Static var compensators

Variables

$P^{\mathrm{G}}_{\mathrm{buy},i,t}$	Purchasing gas
$P^{\mathrm{PVc}}_{i,t}$	Solar power output
$P^{\mathrm{Wc}}_{i,t}$	Wind power output
$P^{\mathrm{grid}}_{i,t}$	The electric power between the microgrid and the distribution network liaison line
$P^{\mathrm{pcc}}_{i,t}$	The gas power between the microgrid interacts with the superior distribution network
$G^{\mathrm{grid}}_{i,t}$	The interactive natural gas power between microgrid and the natural gas supply pipeline
$G^{\mathrm{pcc}}_{i,t}$	The gas power between the microgrid interacts with the superior distribution network
$P^{\mathrm{ren}}_{i,t}$	The output of renewable energy
$P^{\mathrm{ES}}_{i,t}$	The operating power of the electricity storage
$P^{\mathrm{dev}}_{i,t}$	The electricity power of the energy coupling and conversion equipment in microgrid
$P^{\mathrm{load}}_{i,t}$	The electricity load
$G^{\mathrm{ES}}_{i,t}$	The operating power of gas storage
$G^{\mathrm{dev}}_{i,t}$	The gas power of the energy coupling and conversion equipment in microgrid
$G^{\mathrm{load}}_{i,t}$	The gas load
$H^{\mathrm{ES}}_{i,t}$	The operating power of heat storage
$H^{\mathrm{dev}}_{i,t}$	The heat power of the energy coupling and conversion equipment in microgrid
$H^{\mathrm{load}}_{i,t}$	Heat load
H^{GB}_{t}	The thermal power of the gas boiler

H_t^{EB}	The heat generation power of electric boiler
G_t^{P2G}	The gas power of power-to-gas
P_t^{CHP}	The generation power of combined heat and power
P_t^{ESc}	Charging power of the electric energy storage
P_t^{ESd}	Discharging power of the electric energy storage
$Q_{i,t}^{n}$	Reactive power compensation equipment power

References

1. Wu X, Zhang L, Xu Y, Wang S, Guerrero JM. Hierarchical and distributed control of AC and DC microgrid clusters interconnected by flexible DC distribution network. CSEE J Power Energy Syst. 2025:1–12. doi:10.17775/CSEEJPES.2024.01190.
2. Jin J, Sun G, Chen S, Li Y, Liao Y, Mao W, et al. A multi-agent robust deep reinforcement learning approach for coordination of power distribution networks and microgrids with limited information exchange. J Mod Power Syst Clean Energy. 2025:1–12. doi:10.35833/MPCE.2025.000035.
3. Wang Q, Wu W, Sun D, Lin C, Shen Y, Yang Y, et al. A spherical manifold-based optimization method for coordinated operation of active distribution network with networked microgrids. IEEE Trans Smart Grid. 2025:1. doi:10.1109/tsg.2025.3629824.
4. Gao H, Yang J, He S, Liu J. Peer-to-peer electricity sharing for transactive microgrids considering interaction with distribution network operation. CSEE J Power Energy Syst. 2024:1–12. doi:10.17775/CSEEJPES.2023.00860.
5. Li H, Ren Z, Trivedi A, Srinivasan D, Liu P. Optimal planning of dual-zero microgrid on an island toward net-zero carbon emission. IEEE Trans Smart Grid. 2024;15(2):1243–57. doi:10.1109/TSG.2023.3299639.
6. Zou Y, Xu Y, Zhang C. A risk-averse adaptive stochastic optimization method for transactive energy management of a multi-energy microgrid. IEEE Trans Sustain Energy. 2023;14(3):1599–611. doi:10.1109/TSTE.2023.3240184.
7. Liu C, Wang Y, Zou Y, Cui Q. Risk-aware operation of offshore multi-energy microgrids using large-language-model assisted distributed pareto-optimal reinforcement learning. CSEE J Power Energy Syst. 2025:1–12. doi:10.17775/CSEEJPES.2025.02340.
8. Gao G, Yao J, Yang S, Li Y, Zhu K, Yan J. Research on multi-stage optimal dispatch strategy of microgrids with multi-resource clusters based on hybrid data-driven method. CSEE J Power Energy Syst. 2025:1–12. doi:10.17775/CSEEJPES.2024.08040.
9. Zhang H, Li Y, Li T, Wang G, Yue D, Hancke GP. Reputation attack detection based resilient distributed energy management of cyber-physical microgrid. IEEE Trans Smart Grid. 2025;PP(99):1. doi:10.1109/TSG.2025.3632341.
10. Shi W, Xie X, Chu CC, Gadh R. Distributed optimal energy management in microgrids. IEEE Trans Smart Grid. 2015;6(3):1137–46. doi:10.1109/TSG.2014.2373150.
11. Chen Y, Park B, Kou X, Hu M, Dong J, Li F, et al. A comparison study on trading behavior and profit distribution in local energy transaction games. Appl Energy. 2020;280:115941. doi:10.1016/j.apenergy.2020.115941.
12. Tushar W, Yuen C, Mohsenian-Rad H, Saha T, Poor HV, Wood KL. Transforming energy networks via peer-to-peer energy trading: the potential of game-theoretic approaches. IEEE Signal Process Mag. 2018;35(4):90–111. doi:10.1109/MSP.2018.2818327.
13. Zhou Y, Wu J, Long C, Ming W. State-of-the-art analysis and perspectives for peer-to-peer energy trading. Engineering. 2020;6(7):739–53. doi:10.1016/j.eng.2020.06.002.
14. Toutounchi AN, Seyedshenava S, Contreras J, Akbarimajd A. A stochastic bilevel model to manage active distribution networks with multi-microgrids. IEEE Syst J. 2019;13(4):4190–9. doi:10.1109/JSYST.2018.2890062.
15. Liu Y, Guo L, Wang C. A robust operation-based scheduling optimization for smart distribution networks with multi-microgrids. Appl Energy. 2018;228:130–40. doi:10.1016/j.apenergy.2018.04.087.
16. DorMohammadi S, Rais-Rohani M. Exponential penalty function formulation for multilevel optimization using the analytical target cascading framework. Struct Multidiscip Optim. 2013;47(4):599–612. doi:10.1007/s00158-012-0861-x.
17. Li J, Fang J, Zeng Q, Chen Z. Optimal operation of the integrated electrical and heating systems to accommodate the intermittent renewable sources. Appl Energy. 2016;167:244–54. doi:10.1016/j.apenergy.2015.10.054.

18. Thang VV, Ha T, Li Q, Zhang Y. Stochastic optimization in multi-energy hub system operation considering solar energy resource and demand response. Int J Electr Power Energy Syst. 2022;141:108132. doi:10.1016/j.ijepes.2022.108132.
19. Xie M, Ji X, Hu X, Cheng P, Du Y, Liu M. Autonomous optimized economic dispatch of active distribution system with multi-microgrids. Energy. 2018;153:479–89. doi:10.1016/j.energy.2018.04.021.
20. Li Y, Li R, Shi L, Wu F, Zhou J, Liu J, et al. Adjustable capability evaluation of integrated energy systems considering demand response and economic constraints. Energies. 2023;16(24):8048. doi:10.3390/en16248048.
21. Zhou J, Li R, Li Y, Shi L. Aggregation modeling for integrated energy systems based on chance-constrained optimization. Processes. 2024;12(12):2672. doi:10.3390/pr12122672.